Icarus 362 (2021) 114404

Contents lists available at ScienceDirect

Icarus

journal homepage: www.elsevier.com/locate/icarus

The climatology of carbon monoxide on Mars as observed by NOMAD nadir-geometry observations

Michael D. Smith [a,*], Frank Daerden [b], Lori Neary [b], Alain S.J. Khayat [a,c], James A. Holmes [d], Manish R. Patel [d,e], Geronimo Villanueva [a], Giuliano Liuzzi [a,f], Ian R. Thomas [b], Bojan Ristic [b], Giancarlo Bellucci [g], Jose Juan Lopez-Moreno [h], Ann Carine Vandaele [b]

[a] NASA Goddard Space Flight Center, Greenbelt, MD, United States
[b] Royal Belgian Institute for Space Aeronomy, Brussels, Belgium
[c] University of Maryland, College Park, MD, United States
[d] School of Physical Sciences, The Open University, Milton Keynes, United Kingdom
[e] Space Science and Technology Department, Science and Technology Facilities Council, Rutherford Appleton Laboratory, Oxfordshire, United Kingdom
[f] American University, Washington, DC, United States
[g] Instituto di Astrofisica e Planetologia Spaziali, INAF, Rome, Italy
[h] Instituto de Astrofisica de Andalucia, CSIC, Granada, Spain

A B S T R A C T

More than a full Martian year of observations have now been made by the Nadir Occultation for MArs Discovery (NOMAD) instrument suite on-board the ExoMars Trace Gas Orbiter. Radiative transfer modeling of NOMAD observations taken in the nadir geometry enable the seasonal and global-scale variations of carbon monoxide gas in the Martian atmosphere to be characterized. These retrievals show the column-averaged volume mixing ratio of carbon monoxide to be about 800 ppmv, with significant variations at high latitudes caused by the condensation and sublimation of the background CO_2 gas. Near summer solstice in each hemisphere, the CO volume mixing ratio falls to 400 ppmv in the south and 600 ppmv in the north. At low latitudes, carbon monoxide volume mixing ratio inversely follows the annual cycle of surface pressure. Comparison of our retrieved CO volume mixing ratio against that computed by the GEM-Mars general circulation model reveals a good match in their respective seasonal and spatial trends, and can provide insight into the physical processes that control the distribution of CO gas in the current Martian atmosphere.

1. Introduction

Carbon monoxide is a minor constituent in the Martian atmosphere, but it plays an important role in the photochemical cycle of CO_2 production and loss, and it serves as an important tracer for atmospheric circulation patterns (see Lefèvre and Krasnopolsky, 2017 and references therein for a review). As a non-condensable gas, the volume mixing ratio (vmr) of CO is expected to have seasonal and spatial variations on a global and seasonal scale (e.g., Forget et al., 2008; Daerden et al., 2019). Therefore, the seasonal and spatial variation of CO vmr provides a key observational constraint for understanding the dynamical and photochemical processes that operate in the current Martian atmosphere.

Since its initial detection by Kaplan et al. (1969) using high spectral resolution infrared spectroscopy, carbon monoxide has been observed in the Martian atmosphere by a number of ground-based observers at infrared, millimeter, and sub-millimeter wavelengths (e.g., Clancy et al., 1983, 1990; Lellouch et al., 1991; Krasnopolsky, 2003, 2007; Moreno et al., 2009). These observations had limited seasonal and latitudinal coverage, but were able to establish an average CO vmr near 800 ppmv and to identify some latitudinal gradients.

Spacecraft observations have provided more information in greater detail about the seasonal and spatial distribution of CO vmr. Retrievals using observations from the OMEGA (Encrenaz et al., 2006) and PFS (Billebaud et al., 2009; Sindoni et al., 2011) instruments on-board the Mars Express spacecraft explored the variation of CO vmr for certain locations and seasons, while a more complete climatology of CO vmr was characterized using near-infrared observations made by the CRISM instrument on-board the Mars Reconnaissance Orbiter (Smith et al., 2009, 2018) and using new retrievals from the PFS observations (Bouche et al., 2021). These works confirmed a global average CO vmr of about 800 ppmv and revealed the seasonal and spatial patterns expected for a non-condensable gas, including relatively low CO vmr at the summertime poles and an anticorrelation with the annual cycle of surface pressure at low latitudes. Spacecraft observations of CO have been

* Corresponding author at. NASA Goddard Space Flight Center, Greenbelt, MD 20771, United States.
E-mail address: Michael.D.Smith@nasa.gov (M.D. Smith).

https://doi.org/10.1016/j.icarus.2021.114404
Received 29 October 2020; Received in revised form 19 February 2021; Accepted 26 February 2021
Available online 5 March 2021
0019-1035/Published by Elsevier Inc.

combined with general circulation models through data assimilation to demonstrate the capability of models in forecasting the atmospheric state (Holmes et al., 2019).

New near-infrared spectra taken in the nadir geometry by the Nadir Occultation for MArs Discovery (NOMAD) instrument suite (Vandaele et al., 2015, 2018) on-board the ExoMars Trace Gas Orbiter contain the clear spectral signature of multiple CO absorption lines and enable the further characterization and refinement of the CO climatology observed by previous missions. In this paper we present a new climatology of CO vmr based on radiative transfer modeling of the NOMAD nadir-geometry observations of CO. These retrievals provide an independent dataset for comparison against the results found by CRISM and PFS, as well as new information about possible diurnal variations. We also compare our retrievals of CO vmr against the results computed using the GEM-Mars general circulation model (Daerden et al., 2015; Neary and Daerden, 2018; Daerden et al., 2019) to put our results into context and to identify the physical processes responsible for the observed trends in the CO climatology.

In Section 2, we describe the NOMAD instrument and the observations used in this study. In Section 3 we provide details about the retrieval algorithm including the assumptions used and the expected uncertainties in the retrieved quantities. The retrieval results are discussed in Section 4, and in Section 5 we compare the retrieved values against the output from the GEM-Mars general circulation model. Finally, we summarize our findings in Section 6.

2. Data set

2.1. NOMAD instrument

The NOMAD instrument suite was selected for the ExoMars Trace Gas Orbiter mission in order to provide a spectroscopic survey of the Martian atmosphere that would advance our knowledge of the composition of the Mars atmosphere (Vandaele et al., 2015, 2018). The first results from the analysis of NOMAD observations have already been used to (among other things) set new stringent upper limits on methane abundance (Korablev et al., 2019) and to evaluate the impact of Mars global dust storms on the D/H ratio (Vandaele et al., 2019) and the vertical distribution of water vapor (Aoki et al., 2019).

NOMAD consists of three different spectrometers that cover large portions of the ultraviolet, visible, and near-infrared spectral ranges from 0.2 to 4.3 μm. The UVIS (Ultraviolet and Visible Spectrometer) covers the spectral range from 200 to 650 nm (Patel et al., 2017), while the SO (Solar Occultation) spectrometer is dedicated to solar occultation observations at near-infrared wavelengths (2.3–4.3 μm). In this study, we use the spectra taken by the LNO (Limb Nadir and solar Occultation) spectrometer, which can be used in both nadir-viewing and limb-viewing geometries, as well as for solar occultations.

The LNO spectrometer is a modified version of the SOIR (Solar Occultation in the IR) instrument (Nevejans et al., 2006) that was flown on Venus Express (Titov et al., 2006). It uses an echelle grating in combination with an Acousto-Optical Tunable Filter (AOTF) to sample the spectral range from 2.3–3.8 μm at a spectral resolving power of roughly 10,000 (~0.4 cm^{-1}). For each LNO observation, 320 spectral channels cover a spectral range between 20 and 35 cm^{-1} depending on the diffraction order. Each order is characterized by a specific central wavelength, which is selected by the AOTF. A couple dozen different grating orders are used regularly to monitor different atmospheric constituents, including carbon monoxide.

2.2. Observations used for this study

For this work we use all NOMAD LNO observations taken using grating orders 189 and 190 (4250–4300 cm^{-1}, or 2325–2350 nm), which are used specifically to monitor carbon monoxide. Although solar occultation observations have greater sensitivity and enable the vertical distribution to be retrieved, the nadir-geometry observations used here have the advantage of higher horizontal spatial resolution and much more complete seasonal and (horizontal) spatial coverage. Where available, the LNO observations consist of north-south strips across the entire visible disk of Mars containing up to a couple hundred individual spectra for each orbit. The projected instantaneous LNO footprint on the surface of Mars is approximately 0.5 × 17 km (Vandaele et al., 2015), and observations are typically spaced every ~0.7° of latitude along the orbit track. At the near-IR wavelengths used here we depend on reflected solar light for our signal and the contribution from thermal radiation is negligible. Therefore, we cannot retrieve carbon monoxide for nighttime or winter polar regions, and in addition, observations with solar incidence angle greater than 55° are not used because of their low signal-to-noise.

The NOMAD LNO observations used in this study cover the time period between Mars Year (MY) 34, $L_s = 150°$ and MY 35, $L_s = 241°$ (28 March 2018 and 18 July 2020). This time period covers more than a complete Mars Year, with overlapping coverage between two Mars Years during the peak dustiest season when some observations were not used because of excessive atmospheric dust loading (see Section 3.4).

Fig. 1 shows the coverage of the 109,159 retrievals used in this work as a function of season (L_s) and latitude. During each period of time when nadir observations are possible (each lobe in Fig. 1) the local time of the observations changes systematically from late afternoon to early morning. The solar incidence angle is lowest in the center and increases outward to the edge of each lobe. Observations were taken sufficiently often to enable a good characterization of the seasonal and global-scale trends in carbon monoxide volume mixing ratio, but are not capable of

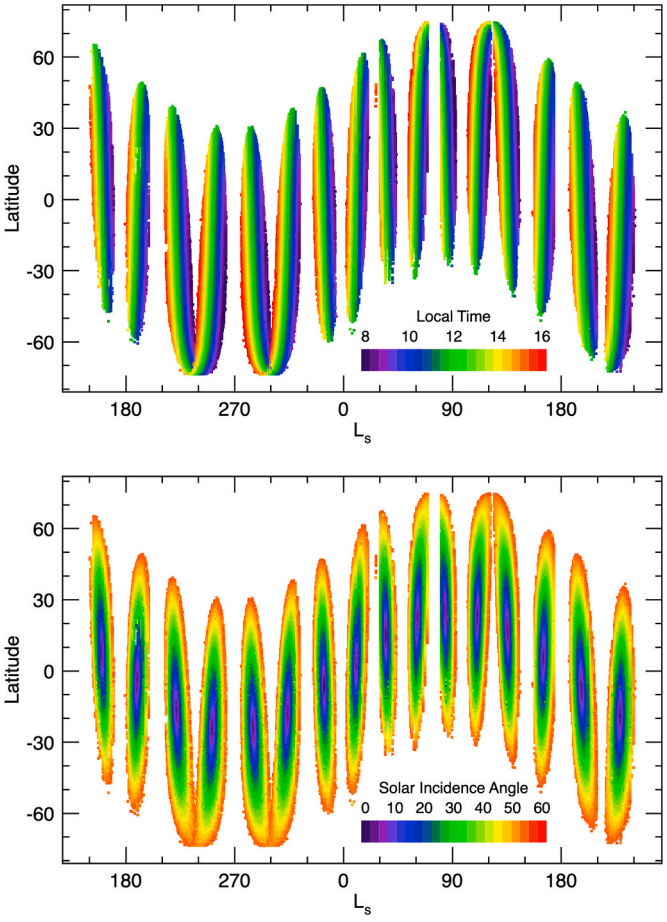

Fig. 1. The seasonal and latitudinal coverage of the NOMAD LNO observations in orders 189 and 190 used in this study. Shown are (top) the local true solar time for each observation, and (bottom) the solar incidence angle.

providing maps on short timescales on the order of days or weeks. Observations using both NOMAD grating orders 189 and 190 were taken throughout the time period shown in Fig. 1.

A typical set of spectra taken using order 190 on one orbit is shown in Fig. 2. In this image each spectrum is represented by a horizontal row in the image with colour indicating the observed signal. The quantity that is shown here and that is used in this analysis is the "Reflectance Factor" field provided by the nominal NOMAD data pipeline processing (further detail about the calibration of NOMAD data can be found in Liuzzi et al., 2019; Thomas et al., 2020). This divides the observed radiance of Mars by the observed solar reference spectrum with corrections for the Mars-Sun distance and mean solar incidence angle. The wavelength of each NOMAD channel depends on the instrument temperature at the time of each measurement (e.g., Liuzzi et al., 2019), so a wavelength correction is performed for each individual observation as a part of the retrieval by fitting the observed lines to their known wavelengths. The individual absorption lines caused by CO are readily apparent as vertical bands in Fig. 2 (for example, at 4285.0, 4288.3, and 4291.5 cm^{-1}).

3. Retrieval algorithm

We use seven lines for the retrieval of carbon monoxide using NOMAD LNO observations from the (2–0) ro-vibrational band, with four lines from order 189 (R0, R1, R2, and R3) and three from order 190 (R6, R7, and R8). As shown in Fig. 3, the CO absorption lines in this spectral region are very well separated from each other and from any other significant absorptions from water vapor or CO_2. At the spectral resolution of the LNO observations, the absorptions have a depth that is typically at a level of 5–10% of the continuum level, which is more than sufficient for a reliable retrieval. These CO lines are part of the same absorption band used for retrievals of CO by the CRISM instrument (Smith et al., 2009, 2018).

3.1. Radiative transfer and assumptions

The radiative transfer modeling used here for computing synthetic spectra of carbon monoxide is essentially the same as that used in our previous retrievals using CRISM spectra (Smith et al., 2009, 2018). To perform the retrieval, radiative transfer modeling is used to compute an expected spectrum for a given volume mixing ratio of carbon monoxide, and that CO vmr is then varied until the resulting integrated line depth of the CO absorptions in the computed spectrum matches that from the observed NOMAD LNO spectrum.

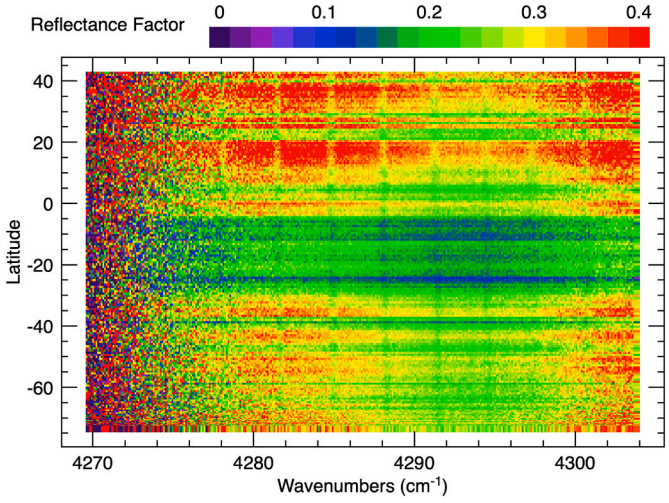

Fig. 2. A typical NOMAD LNO observation for order 190 shown in terms of reflectance factor. The data were taken on 5 November 2018 (MY 34, Ls = 283°). Spectral features caused by CO are visible as vertical lines in the image. In this representation, the continuum level signal is controlled largely by surface albedo, solar incidence angle, and aerosol scattering.

The radiative transfer is modeled using the discrete ordinates approach (e.g., Goody and Yung, 1989; Thomas and Stamnes, 1999), which explicitly includes multiple scattering by aerosols. Absorption of carbon monoxide gas is computed using the correlated-k approximation (Lacis and Oinas, 1991), using the latest version of the HITRAN spectroscopic database for line parameters, which now include line broadening from carbon dioxide (Gordon et al., 2017). The viewing geometry, including the solar incidence angle, the emergence angle, and phase angle are read from spacecraft records and are assumed to be known quantities.

The thermal state of the atmosphere for each observation is provided by the OpenMARS database, which is a reanalysis product that combines spacecraft observations with a Mars General Circulation Model (Holmes et al., 2020). Thus, the temperature profiles read from OpenMARS and used in this work include the effects of the global dust storm that occurred during Mars Year 34 (e.g., Guzewich et al., 2018; Smith, 2019). Surface pressure is taken from the Mars Climate Database v.5.3 (Forget et al., 1999; Millour et al., 2018) using its high-resolution setting to resolve sub-grid topography. Surface albedo is taken from a map based on Thermal Emission Spectrometer observations (Christensen et al., 2001).

Scattering from dust and water ice aerosols affects the observed depth of gas absorptions and must be included in the model for an accurate retrieval. The optical depth of dust and water ice aerosols for each NOMAD LNO spectrum is estimated from concurrent observations by the THEMIS instrument on Mars Odyssey (Smith, 2018, 2019). The scattering properties of dust and water ice aerosols are taken from the analysis of CRISM near-infrared observations (Wolff et al., 2009), while the aerosol particle size (effective radius of 1.5 μm for dust and 2.0 μm for water ice) is an average value from the analysis of many previous spacecraft observations (e.g., Wolff and Clancy, 2003; Clancy et al., 2003; Wolff et al., 2006, 2009; Vincente-Retortillo et al., 2017). The dust aerosol is assumed here to be well-mixed with the background atmosphere. Water ice aerosol is assumed to form clouds above the water condensation level, with no cloud below and a well-mixed cloud above. Discussion of the uncertainties related to the above assumptions is presented in Section 3.4.

3.2. Retrieval algorithm process

Fig. 4 shows representative averaged NOMAD LNO spectra for the seven lines chosen for the retrieval. The center locations for these lines for order 189 are: 4263.8, 4267.5, 4271.2, and 4274.7 cm^{-1}, and for order 190 are: 4285.0, 4288.3, and 4291.5 cm^{-1}. For each line, we divide the observed reflectance factor by the continuum level and compute the total integrated line depth for the line. The integrated line depth retains all the information from the line since these lines are spectrally unresolved in the observations. The observation to be fit is then the sum of the integrated line depths for all of the lines in each spectrum.

The retrieved value of CO volume mixing ratio is determined by computing synthetic spectra with a given CO vmr and computing the integrated line depth for the three or four lines in the computed spectrum (with the continuum divided out) in the same way as done for the observation. In the computation, CO is assumed to be well-mixed vertically, which is supported by previous studies (e.g., Smith et al., 2018) and by model results for the lower part of the atmosphere where most of the CO molecules lie (e.g., Daerden et al., 2019). The final retrieved value of CO vmr is simply that value where the computed integrated line depth matches the observed value.

Using this algorithm makes the retrieval robust to uncertainties in the instrumental spectral response function and to errors or uncertainties in the overall calibration of the observed reflectance factor. The drawback of using integrated line depth as a metric is its sensitivity

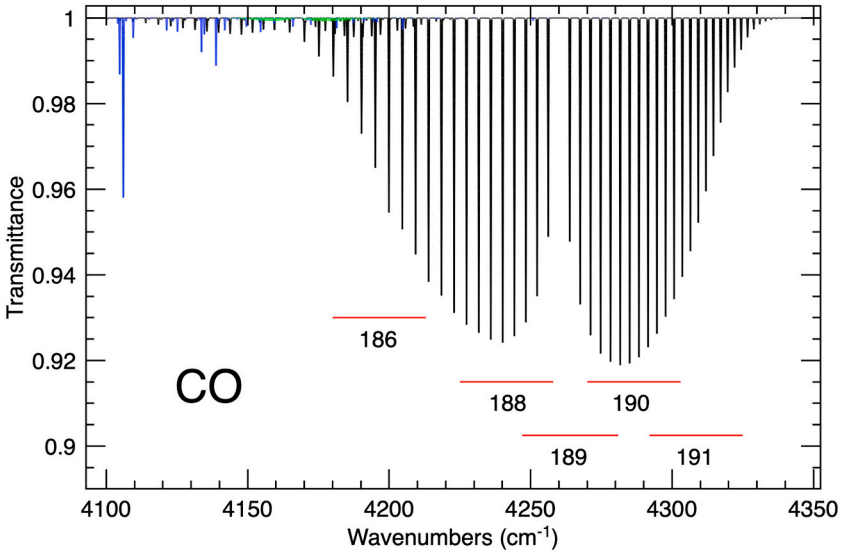

Fig. 3. A computed spectrum of the absorptions from CO (black), water vapor (blue), and CO_2 (green) convolved to a spectral resolution of 0.4 cm^{-1}. The spectral range covered by different NOMAD LNO grating orders are indicated by the numbers 186 through 191. The orders used in this study (189 and 190) contain strong CO lines with no interference from other gases. (For interpretation of the references to colour in this figure legend, the reader is referred to the web version of this article.)

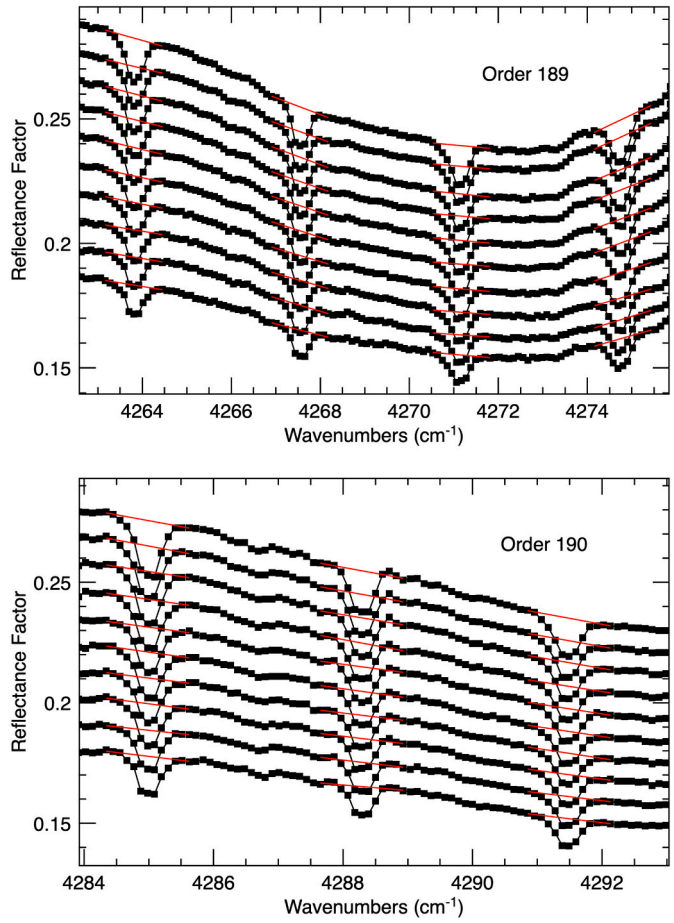

Fig. 4. Averaged spectra for (top) order 189 and (bottom) order 190 showing the CO absorptions used for the retrieval. These are lines from the (2–0) ro-vibrational band of CO, lines R0, R1, R2, and R3 for order 189, and R6, R7, and R8 for order 190. The red line segments show the estimated continua and the spectral range over which the integrated line depths are computed for each line. (For interpretation of the references to colour in this figure legend, the reader is referred to the web version of this article.)

to the choice of the continuum. To minimize this sensitivity, we define the continuum as being linear in reflectance factor and computed using spectral channels that are the same constant distance (plus and minus 6 LNO channels, or about ±0.64 cm^{-1}) from the line center for each line. These computed continua are shown in Fig. 4 as red line segments.

Along with the retrieved value of CO vmr, for each spectrum we also record the observed noise level in the observation by computing the root mean square (rms) variation of the reflectance factor in the spectral regions between the lines used in the retrieval. This quantity is used as a quality control parameter. Retrievals with a noise level greater than a threshold value are rejected.

3.3. *Modeling the AOTF*

The presence of the AOTF complicates modeling of the observed NOMAD spectrum since the observed signal for a given diffraction order will also contain some amount of signal from neighboring orders. Since the CO absorption lines used for this analysis are well spaced with essentially no contribution from other species (Fig. 3), the main concern is the addition of continuum signal from neighboring orders to the observed signal of the CO lines in the orders being studied. The effect of adding this continuum from neighboring orders would be to artificially reduce the integrated line depth that we use as our observation to be retrieved, and thus to systematically reduce the CO vmr values that we retrieve.

Fortunately, this effect is observed to be relatively small for the NOMAD LNO observations in orders 189 and 190 that are used for our CO retrievals. Ideally, absorptions that are very optically thick at the spectral resolution of NOMAD would be used to estimate this out-of-order continuum contribution. In this case, the expected signal would be zero inside the absorption and any non-zero signal that is observed could be attributed to the continuum from other orders. There are no such optically thick absorptions for these diffraction orders, so instead we use two different means to estimate the contribution from neighboring orders.

The most straightforward method is to look at the relative amplitude of spectral lines aliased from neighboring orders by the AOTF. Fig. 5 shows four of the same spectra for order 189 as shown in Fig. 4. The black vertical lines indicate the frequency of the CO absorptions for order 189. As expected, they line up with the observed spectral features. The red and blue vertical lines indicate the frequencies where we would expect to see CO absorptions aliased from orders 188 (red lines) and 190 (blue lines) by the AOTF. Spectral features aliased from neighboring

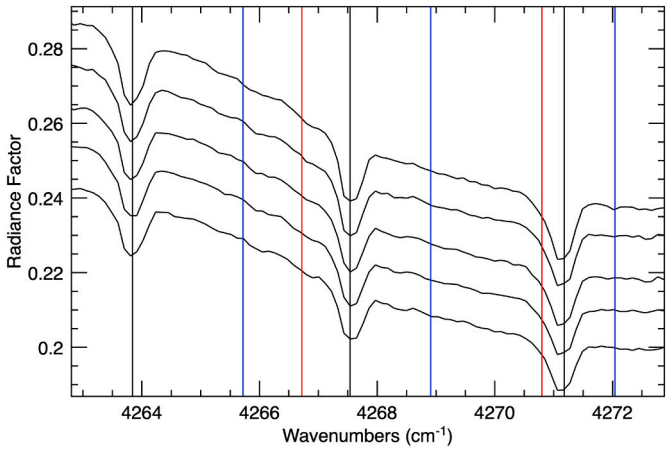

Fig. 5. Averaged spectra for order 189 showing the expected spectral locations of spectral features. The black vertical lines show the frequencies of three of the main CO lines in order 189. The red and blue vertical lines show the frequencies where CO absorptions from orders 188 (red) and 190 (blue) would appear if aliased by the AOTF. (For interpretation of the references to colour in this figure legend, the reader is referred to the web version of this article.)

orders are clearly visible in many NOMAD observations, for example, the solar occultation observations analyzed by Aoki et al. (2019), and the analysis of Liuzzi et al. (2019). However, the LNO observations for orders 189 and 190 show essentially no features at the expected locations, which indicates that the contribution from other orders is small.

The top panel of Fig. 6 shows how comparing the observed line depth of a CO absorption aliased from a neighboring order (4268.8 cm-1, the middle blue line in Fig. 5) against the observed line depth of a CO absorption from the order being observed (4267.55 cm-1, the middle black line in Fig. 5) can be used to estimate the continuum contribution from neighboring orders. The greater the observed line depth ratio, the greater the contribution from neighboring orders, and the smaller the line depth would be for the CO lines used in the retrieval. A detailed analysis looking at all the LNO order 189 observations shows this observed line depth ratio to be no larger than 0.02. Using Fig. 6, this implies that the observed CO lines used in this retrieval are at least 0.92 times as strong as they would be with no AOTF. In other words, the true CO line depths at Mars (with no AOTF) are at most 1.08 times stronger than observed.

A second way to estimate the out-of-order continuum contribution is to look at how retrieved CO varies as a function of a known quantity where the expected variation is non-linear. The variation of CO with surface pressure is the best example of this. Surface pressure is (essentially) known from model results, and the expected line depth of CO varies non-linearly with surface pressure both because the curve of growth is non-linear (i.e., doubling the amount of CO leads to a line depth less than twice as large) and because of the effects of pressure broadening of the absorption lines.

The bottom panel of Fig. 6 shows the results of a numerical experiment where we use a constant CO vmr and a range of surface pressures to compute expected line depths. We multiply each of these line depths by factors ranging from 0.9 to 1.0 (as indicated in Fig. 6 by the numbers at the ends of the black curves) and then perform the retrieval on these reduced "observed" line depths assuming no AOTF. The results, normalized to their value at 6 mbar, show a systematic variation with surface pressure. The actual CO retrievals using NOMAD LNO observations (presented in detail in Section 4) for orders 189 and 190 are shown by the red and blue points. Here we have used only retrievals between 30° S and 30° N latitude to minimize real variations of CO vmr, and we have smoothed the results by convolving with a function 1 mbar wide in surface pressure. As expected, the retrievals do show a tendency toward lower CO vmr values at lower surface pressures, but the implied

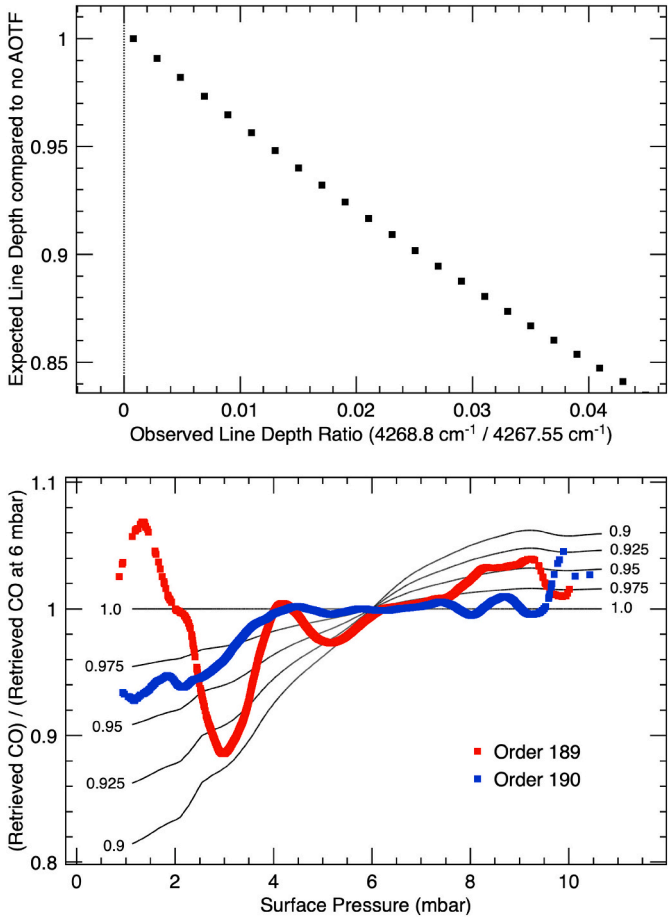

Fig. 6. Two ways to estimate the continuum contribution from neighboring orders from the AOTF. (Top panel) The expected line depth of CO lines as a fraction of that with no AOTF is shown as a function of the observed line depth of a CO absorption aliased from a neighboring order (4268.8 cm-1, the middle blue line in Fig. 5) against the observed line depth of a CO absorption from the order being observed (4267.55 cm-1, the middle black line in Fig. 5). (Bottom panel) For line depths multiplied by a given constant value (the numbers given at each end of the black lines), the retrieved CO vmr as a function of surface pressure has a systematic variation as shown by the black curves. The CO vmr retrieved from the observations (red and blue points) are consistent with this factor being 0.95 or greater. (For interpretation of the references to colour in this figure legend, the reader is referred to the web version of this article.)

continuum contribution from other orders is not large, with the resulting strength of the observed CO lines being at least 0.95 times as strong as they would be with no AOTF.

Taken together, the two independent analyses above present strong evidence that the AOTF contribution to the continuum from neighboring orders is relatively minor for the specific case of the LNO observations for orders 189 and 190. Again, we note that AOTF is observed to produce significant contributions from neighboring orders for other orders and modes (e.g., Liuzzi et al., 2019; Aoki et al., 2019). For this case of these retrievals, the observations are consistent with the CO lines being at least 0.92–0.95 times as strong as they would be with no AOTF. Therefore, for simplicity we have chosen to not include the AOTF in our retrieval. Systematically underestimating line depths by 5–8% would lead to a systematic underestimate of retrieved CO by as much as 20%. However, any such effect of the AOTF not accounted for in the retrieval would be a nearly constant factor applied to every individual retrieval, so that while this uncertainty would affect the overall average CO vmr it would have essentially no effect on the seasonal and latitudinal variations of CO that are the focus of this work.

3.4. Uncertainties

In addition to uncertainties from the AOTF, there are a number of other sources that could contribute systematic uncertainties. Given the form of our retrieval algorithm, the uncertainty in retrieved results is most easily estimated through the use of numerical experiments. For each source of uncertainty to be evaluated, the retrieval algorithm can be performed over a range of different assumptions, approximations, or values to evaluate the resulting change in the retrieved volume mixing ratio of carbon monoxide.

The most straightforward quantities to test are model-related assumptions, such as the number of vertical layers in the model, the number of radiation streams included in the discrete ordinates formulation, and the number of terms kept in the Legendre polynomial expansion of the scattering phase functions. These parameters can be set large enough so that they do not contribute significantly to the total uncertainty. In each case the model parameters were chosen so that the retrieved CO vmr changed by less than 1% when the number of model layers, radiation streams, or phase function terms was doubled. The actual values used in the retrieval are 16 radiation streams, 32 terms in the Legendre polynomial expansion, and 25 vertical layers in the model.

Although thermal radiation is negligible in these observations, atmospheric temperatures can still affect the retrievals since the spectroscopic properties of CO, including line strengths and widths, are temperature dependent. Since we use atmospheric temperatures from OpenMARS that are specifically computed from assimilation of observations during Mars Years 34 and 35, we expect them to be well within 10 K of the true value for all cases. As a test of the worst case, we found that an offset in the temperature profile by 10 K over the entire atmosphere leads to a 2–6% change in retrieved CO vmr.

It is not possible to reliably retrieve aerosol optical depth from the individual NOMAD LNO spectra themselves because of the very limited spectral range in each spectral order. However, the use of dust and water ice aerosol optical depth from concurrent THEMIS observations provides a useful estimate. Numerical experiments show that doubling the aerosol optical depth found outside of major dust storms leads to changes in the retrieved CO vmr by 5% or less. During large dust storms the optical depth of the dust can become large enough to effectively screen the lower part of the atmosphere so that the entire column is not sampled by the observations. For this reason, we choose to reject any observation for which the extinction optical depth at 9-μm is greater than unity. This corresponds to an extinction optical depth at the wavelength used in this retrieval of about 1.8. Our assumptions for the vertical profile of dust and water ice aerosol are found by numerical experiment to cause changes in the retrieved values by 10% or less for any reasonable choices.

Uncertainty related to our definition of the continuum level was tested by performing the retrieval for a large suite of cases using different offsets from the line center for computing the continuum (including cases with asymmetric offsets). The retrieval results were found to vary by as much as 10% for reasonable choices for the definition of the continuum. Considering all of the above sources of uncertainty, we estimate that the total systematic one-sigma uncertainty in an individual retrieval of CO vmr to be 20% or less from sources other than the AOTF.

Perhaps the most straightforward way to estimate an overall uncertainty estimate is by looking at the retrieval values themselves. In addition to the uncertainties described above, the amplitude of random noise in the observed spectra relative to the observed continuum level varies significantly as a function of solar incidence angle, surface albedo, and the distance between Mars and the Sun. As mentioned earlier, we compute the amplitude of the random noise relative to the continuum level for each spectrum to use as a quality criterion. We select the maximum allowed value for the noise level based on a tradeoff between the desire to retain as many retrievals as possible, while keeping the observation-to-observation variation of retrieved CO vmr to a minimum.

For a given maximum allowed value for the noise level, we compute the rms difference between individual retrievals and a smoothed average formed by a 2-D convolution of the retained retrievals using a bin size 45° in L_s and 15° in latitude. Fig. 7 shows the results for this analysis, which was performed separately for retrieval results from orders 189 and 190. For the strictest cases (lowest maximum allowed noise level) the fraction of the retrievals retained is low, but the overall uncertainty in the retrievals estimated by the rms from their smoothed average is also relatively low. As the noise level criterion is relaxed to allow retrievals from observations with higher noise levels, progressively more retrievals are retained at the cost of more scatter in the retrieval results. Given the relatively gradual slopes in Fig. 7, we select values (indicated by arrows) for the maximum allowed noise level to retain 85–90% of the retrievals. Specifically, we set the maximum allowed noise level relative to the continuum level to be 0.025 for order 189 and 0.035 for order 190. This leads to our best estimate for the overall uncertainty in individual retrievals of CO vmr to be about 240 ppmv for order 189 and 290 ppmv for order 190. Given that the global, seasonal average is about 800 ppmv (see Section 4), this corresponds to 30–35%, which is comparable to or slightly better than that for the CRISM retrievals of CO vmr (Smith et al., 2009, 2018). This total uncertainty is larger enough than the 20% systematic uncertainty described above that these retrievals are not dominated by systematics.

4. Retrieval results

Here we present the results of the retrieval of the column-integrated carbon monoxide volume mixing ratio for all NOMAD LNO observations using orders 189 and 190 taken between Mars Year (MY) 34, $L_s = 150°$ and MY 35, $L_s = 241°$ (28 March 2018 and 18 July 2020). This covers 1.25 Mars Years, providing a climatological view of CO and its seasonal and spatial variations. Excluded are observations with a solar incidence angle greater than 55°, those taken during major dust storms, and those with noise levels that exceed the threshold value given in the previous section. These retrieval results are available for download at doi:10.17632/px89dk6ck9.1

4.1. Climatology of retrieved carbon monoxide

The retrieved column-integrated carbon monoxide volume mixing ratio is shown in Fig. 8 as a function of season (L_s) and latitude separately for the retrievals using order 189 and 190. As described above in detail, the uncertainty in individual retrieved values are relatively large (30–35%) so the CO vmr shown in Fig. 8 has been smoothed to highlight the trends. The size of the smoothing box is 15° in L_s and 15° in latitude and is shown in the figure for comparison. In total, there are 34,152 retrievals for order 189 and 75,007 retrievals for order 190.

The overall level of CO vmr and its seasonal and latitudinal variations are broadly similar between the two orders. While there are minor differences, perhaps most notably the generally higher CO vmr in order 189 retrieved around $L_s = 180°$, these differences are well within the stated uncertainties and do not appear from our analysis to arise from any systematic differences between the two orders. Therefore, from this point forward we will describe the combined results from each of the two orders under the assumption that this provides the most accurate value possible.

The CO climatology displayed in Fig. 8 bears a strong resemblance to those retrieved previously from CRISM (Smith et al., 2009; Smith, 2019) and from Mars Express PFS (Bouche et al., 2021), and is largely as expected for a non-condensable gas (e.g., Forget et al., 2008; Daerden et al., 2019; Holmes et al., 2019). There is depletion of carbon monoxide in the summertime polar regions in both hemispheres, although it is significantly stronger in the south. The southern hemisphere summertime depletion leads to CO vmr values of 400 ppmv or less poleward of 70°S, while in the north at least ~600 ppmv of CO is maintained at all observed locations. In both hemispheres the minimum CO vmr values

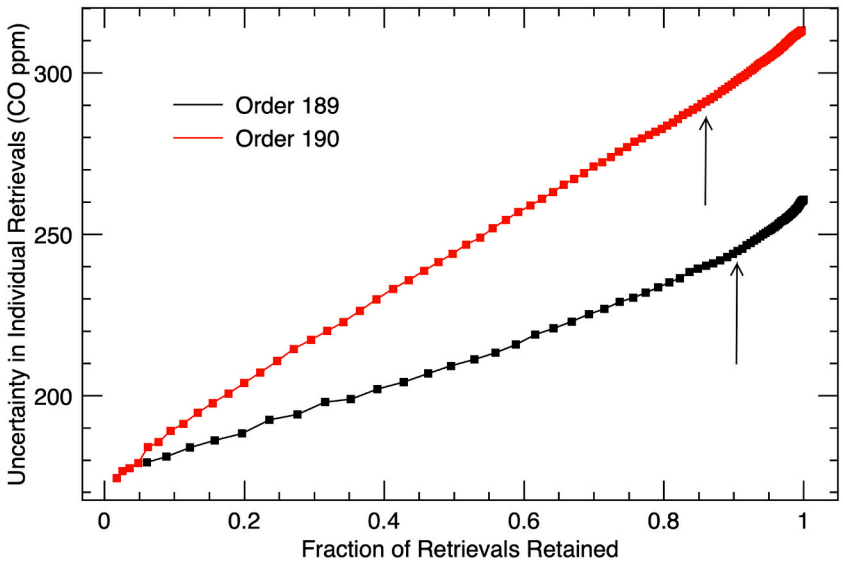

Fig. 7. The observed level of uncertainty in the retrieved value of CO vmr as a function of the fraction of retrievals retained. Each point represents a different upper limit for the maximum allowed noise level in the observations. The arrows show the selected upper limit for each order.

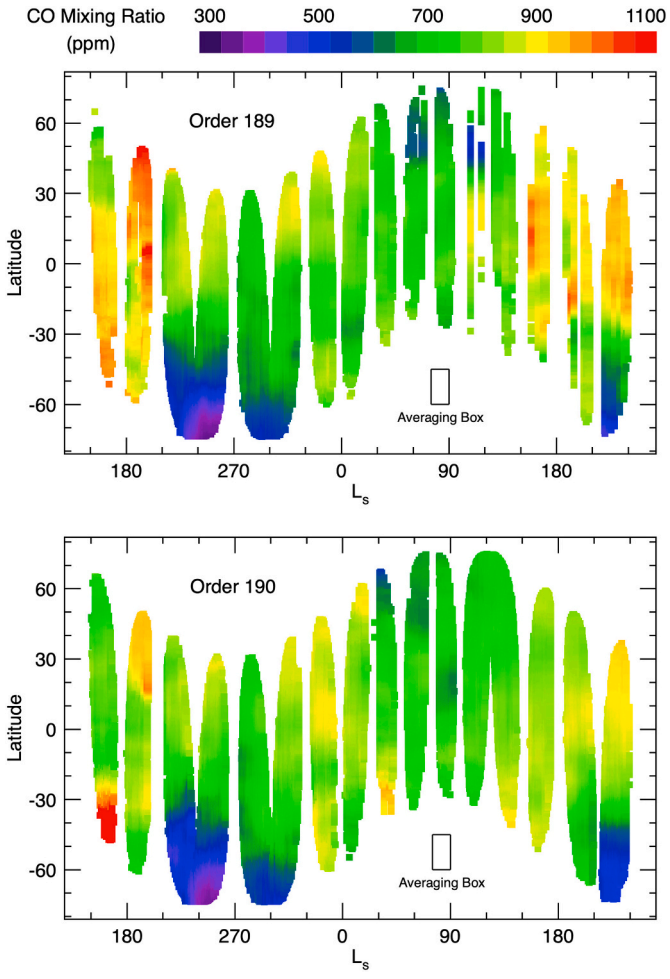

Fig. 8. The column-averaged carbon monoxide volume mixing ratio retrieved from NOMAD LNO spectra as a function of season, latitude, and grating order.

are found somewhat before solstice (by up to ~30° of L_s), especially at latitudes further removed from the pole. The summertime depletion of CO extends to roughly 40° latitude in both hemispheres, with a roughly constant gradient at higher latitudes trending to lower CO vmr toward the pole. Model results indicate a corresponding maximum in CO vmr over the winter poles (Forget et al., 2008; Daerden et al., 2019; Holmes et al., 2019), but this cannot be directly confirmed with retrievals using NOMAD LNO, which rely on solar illumination for the observed signal.

The NOMAD LNO retrievals show that the CO vmr at low latitudes follows a seasonal variation that ranges between roughly 700 ppmv near $L_s = 0°$ and 900–950 ppmv near $L_s = 180°$, with an annually averaged value near 800 ppmv. Moving from south to north, the peak annual value tends to occur at gradually later seasonal dates, from about $L_s = 140°$ at 30° S latitude to about $L_s = 220°$ at 30° N latitude (this trend is more easily seen in the combined and smoothed version of the retrievals discussed in Section 5.1 and shown in Fig. 10). As expected for a non-condensable gas, the overall seasonal variation of CO vmr is observed to roughly follow an inverse relation with the annual variation of surface pressure observed from the surface of Mars (e.g., Tillman et al., 1993; Martínez et al., 2017), although the pattern is also modified by the latitudinal transport of CO (e.g., Daerden et al., 2019; Smith et al., 2018) as will be further discussed in Section 5.2.

Given the relatively long chemical lifetime of CO lived (~6 years; Krasnopolsky, 2007), we do not expect to see interannual variations in these retrievals. The differences between the MY 34 retrievals at the beginning of the time period shown in Fig. 8 and the MY 35 retrievals at the end are instead indicative of the level of uncertainty in the retrievals.

4.2. *Spatial and diurnal variations of retrieved carbon monoxide*

Fig. 9 shows maps of the spatial variation of CO vmr for the four cardinal seasons of the Martian year. To attempt to identify trends, a spatial smoothing has been performed using a box 45° in longitude by 15° in latitude. The largest variations are the latitudinal gradients that describe the annual climatology described in the previous section. At $L_s = 270°$ there is a clear gradient from higher values of CO vmr in the north where it is winter to lower values in the south where it is summer.

Overall, there appears to be limited variation of CO vmr with longitude. The relative lack of correlation between CO vmr and surface topography supports our assumption that CO is largely well-mixed, at least in the lower portion of the atmosphere containing the bulk of the column mass. Most of the small amplitude longitudinal variations that

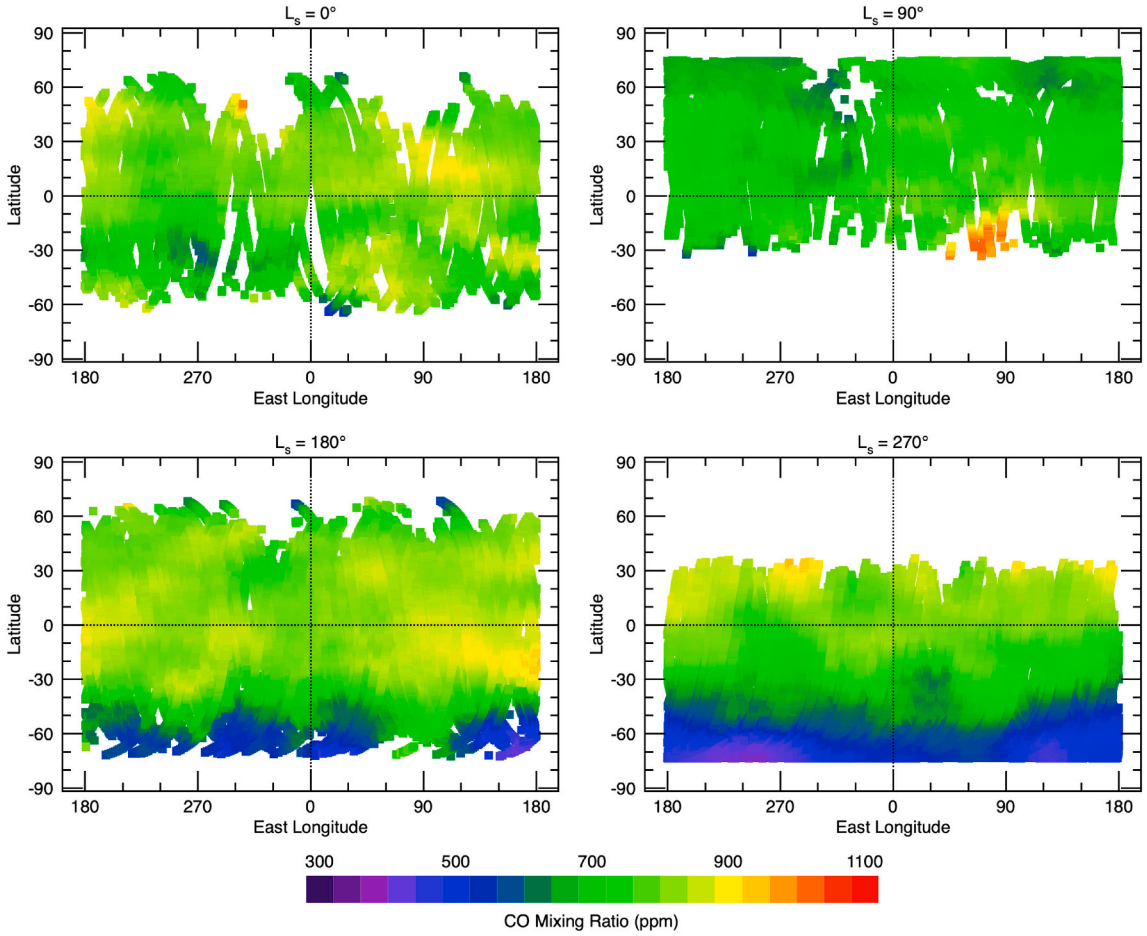

Fig. 9. Maps showing the spatial variation of CO vmr retrieved from NOMAD LNO spectra for four different seasons.

do appear in Fig. 9 are not statistically significant and do not correspond to features in similar maps of CO vmr based on CRISM retrievals presented in Smith et al. (2018). The exception is that the Hellas region at $L_s = 90°$ stands out as having a higher CO vmr than neighboring locations. This enhancement in Hellas during winter was also observed in CRISM retrievals of CO (Smith et al., 2018), although the corresponding enhancements observed in regions with low-lying topography in the north at $L_s = 270°$ are not observed in the LNO retrievals shown here.

Recalling the top panel of Fig. 1, the precessing orbit of the Trace Gas Orbiter enables NOMAD to view a range of local times between roughly 08:00 and 16:00 local true solar time over a relatively short seasonal timescale. However, our analysis of the retrievals does not reveal any systematic variation of column-integrated CO vmr as a function of local time at levels greater than 10%, at least for the daytime hours observable by NOMAD LNO.

5. Discussion

5.1. Comparison with CRISM and other previous results

The retrievals of carbon monoxide volume mixing ratio from this work can be directly compared against previous retrievals from other spacecraft observations. In particular, we focus here on a comparison against the retrievals from CRISM, which use the same CO absorptions and have a similar uncertainty level (Smith et al., 2009, 2018). The CRISM observations were taken from MY 28 to 33. The top two panels in Fig. 10 show a side-by-side comparison of the CO climatology retrieved from CRISM and the current work. For ease of comparison, each has been smoothed with a box 45° in L_s and 15° in latitude to highlight global/seasonal trends, and the CRISM climatology has been resampled to the same L_s and latitude values as given by the NOMAD LNO retrievals.

The overall annual average value is roughly the same in the NOMAD LNO and CRISM retrievals at 800 ppmv. And, the overall pattern of variation described in Section 4.1, with reduced CO vmr near the south pole during summer solstice, a smaller reduction in CO vmr near the north pole during summer solstice, and low-latitude CO vmr inversely correlated with the annual cycle of surface pressure, is observed in both the NOMAD LNO and the CRISM datasets. However, one difference is that the amplitude of the variations is noticeably less in the NOMAD LNO retrievals, being perhaps half as large as that in the CRISM retrievals.

Other differences are present, but smaller. The northern summer minimum in the CRISM retrievals is more extensive than in the NOMAD LNO retrievals, both in terms of latitudinal extent and seasonal duration. On the other hand, the southern summer minimum has very similar latitudinal extent and seasonal duration in the two datasets. The NOMAD LNO retrievals tend toward somewhat greater CO vmr values than those from CRISM at low northern latitudes during the second half of the Martian year ($L_s = 180°$–$360°$) and do not show the slight decrease apparent in CRISM southern hemisphere retrievals between $L_s = 0°$ and 120°.

Recently, another climatology of CO vmr has been retrieved using observations from the Planetary Fourier Spectrometer (PFS) on the Mars Express spacecraft (Bouche et al., 2021) spanning MY 26 to 34. This retrieval uses a different set of CO absorptions at ~2100 cm^{-1} (4.7 μm), but are still directly comparable to the NOMAD LNO results. Bouche et al., 2021 find an overall annual average CO vmr of 820 ppmv and

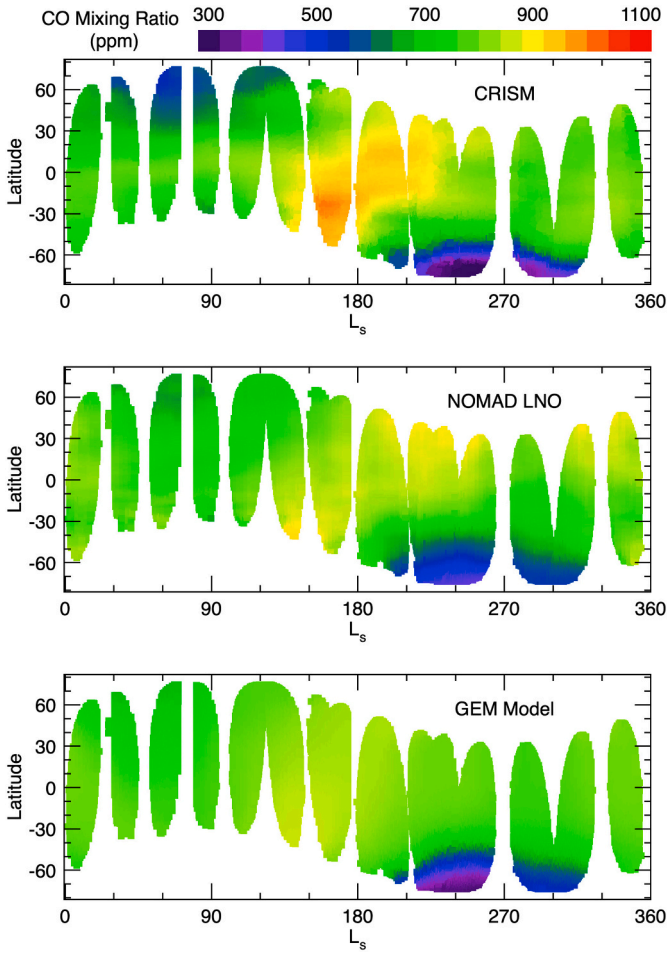

Fig. 10. A comparison of CO vmr climatologies from (top) CRISM, (middle) NOMAD LNO, and (bottom) the GEM-Mars model. The CRISM and GEM-Mars model data have been interpolated to the times and locations of the NOMAD LNO retrievals, and all three datasets have been smoothed (45° in L_s and 15° in latitude) for easier comparison.

many of the same climatological variations described above. Their southern summer minimum has a somewhat smaller amplitude (~500 ppmv for PFS, ~400 ppmv for NOMAD LNO), but the northern summer minimum is somewhat deeper (~600 ppmv for PFS, ~650 ppmv for NOMAD LNO) and there is a larger annual variation at low latitudes in the PFS retrievals.

It is unlikely that the observed differences between the CRISM, PFS, and NOMAD retrievals are caused by real interannual variations in CO vmr. The chemical lifetime for CO is relatively long, and the different retrievals are generally within the uncertainties of the different retrievals. Furthermore, all three of the climatologies compared here (from NOMAD, CRISM, and PFS) are of retrieved values that have been averaged over all Mars Years observed by each instrument.

5.2. Comparison with GCM modeling results

The retrievals of CO vmr from the NOMAD LNO observations can also be compared against model results. Such a comparison can provide insight into the physical processes that drive the observed climatology, and differences between observations and model results can identify areas where improvement is needed in the model or retrieval process.

The model used here is the GEM-Mars General Circulation Model (Daerden et al., 2015; Neary and Daerden, 2018; Daerden et al., 2019). This model uses 103 vertical levels extending from the surface to ~150 km, and it is operated on a grid with a horizontal resolution of 4° × 4° in latitude and longitude. More details on the physical parameterizations in the model and evaluations of simulations are provided in Neary and Daerden (2018), Smith et al. (2018), Daerden et al. (2019), Neary et al. (2020), and Bouche et al., 2021. Here we summarize the parameterization for the non-condensable gas enrichment. Deposition (sublimation) of CO_2 above a model point results in a change of the surface pressure. The dynamical core of the GCM then readjusts the atmospheric mass globally, and the impact of the mass loss at the poles is spread out instantaneously over the entire planet. Locally, the enrichment (or depletion) of minor species will build up more gradually and spread out on a longer timescale by eddy mixing and global circulation. Because of the definition of the model levels in a GCM in terms of surface pressure (implying that the model levels themselves will be modified upon deposition or sublimation), this local process is difficult to disentangle from the global pressure correction. Forget et al. (2008) and Lian et al. (2012) developed methods to treat this problem in their GCMs. In GEM-Mars we apply a simple parameterization that corrects the local vmr after deposition (or sublimation) in two steps. First the vmr of CO_2 is modified at all model levels by a single factor that corrects its column abundance to match the local surface pressure change. Then it is additionally modified at those vertical model levels where CO_2 ice deposition occurred, by a factor that is proportional to the vmr of condensing (or sublimating) ice particles. The factors of proportionality (one for deposition and one for sublimation, see Smith et al. (2018) and Bouche et al., 2021 for details) do not necessarily have the same values, as they describe different processes that involve different timescales, but they should be well balanced to ensure that the total atmospheric content of noncondensing species does not change.

For the simulations presented here, the atmospheric dust was constrained by the dust climatologies provided by Montabone et al. (2015, 2020). For total CO columns, no significant difference was found between using the dust climatology for a year with nominal dust loading (e.g., MY 33) and using the observed dust climatology for MY 34 (when the early NOMAD observations were taken), which included a global dust storm (e.g., Smith, 2019). It was found that the global dust storm had an impact on the higher altitude photochemistry through the redistribution of water vapor (Neary et al., 2020), and therefore also on CO vmr in the upper atmosphere, but did not have an impact on the lower atmospheric CO and on the total column amounts such as retrieved by NOMAD LNO observations.

The bottom two panels of Fig. 10 show a comparison of CO vmr climatology as retrieved by NOMAD LNO observations against that computed by GEM-Mars. Here, the overall average initial value of CO vmr has been adjusted in the model, compared to the results shown in Smith et al. (2018), to match the NOMAD observations, so it is the seasonal and latitudinal variations that should be compared. The GEM-Mars model closely matches the observed climatological patterns. In particular, the southern summer minimum is well represented as is the modest increase in low-latitude CO vmr between $L_s = 120°$ and 210° in response to the annual minimum in surface pressure. The amplitudes of those two features as computed by GEM-Mars are more similar to those observed by NOMAD LNO than to the larger amplitude features observed by CRISM. Perhaps the largest difference between the model and the retrievals is the northern summer minimum. The NOMAD LNO retrievals show a much smaller decrease than the CRISM retrievals, but the minimum in the GEM-Mars has even smaller amplitude.

Fig. 11 shows a comparison between the NOMAD LNO retrievals and the GEM-Mars model results in some more detail. Both datasets have been binned in latitude bands as stated, and then binned in L_s using a box 15° wide sliding 5° of L_s between each point. Again, there is a close correspondence with the largest differences being at high northern latitudes where the model predicts higher CO vmr than observed, and a smaller latitudinal gradient at low latitudes (−40° to +40°) during the second half of the Martian year (L_s = 180°–360°). The remaining differences, with a root-mean-square amplitude of ~50 ppmv, are within the noise level in the retrievals.

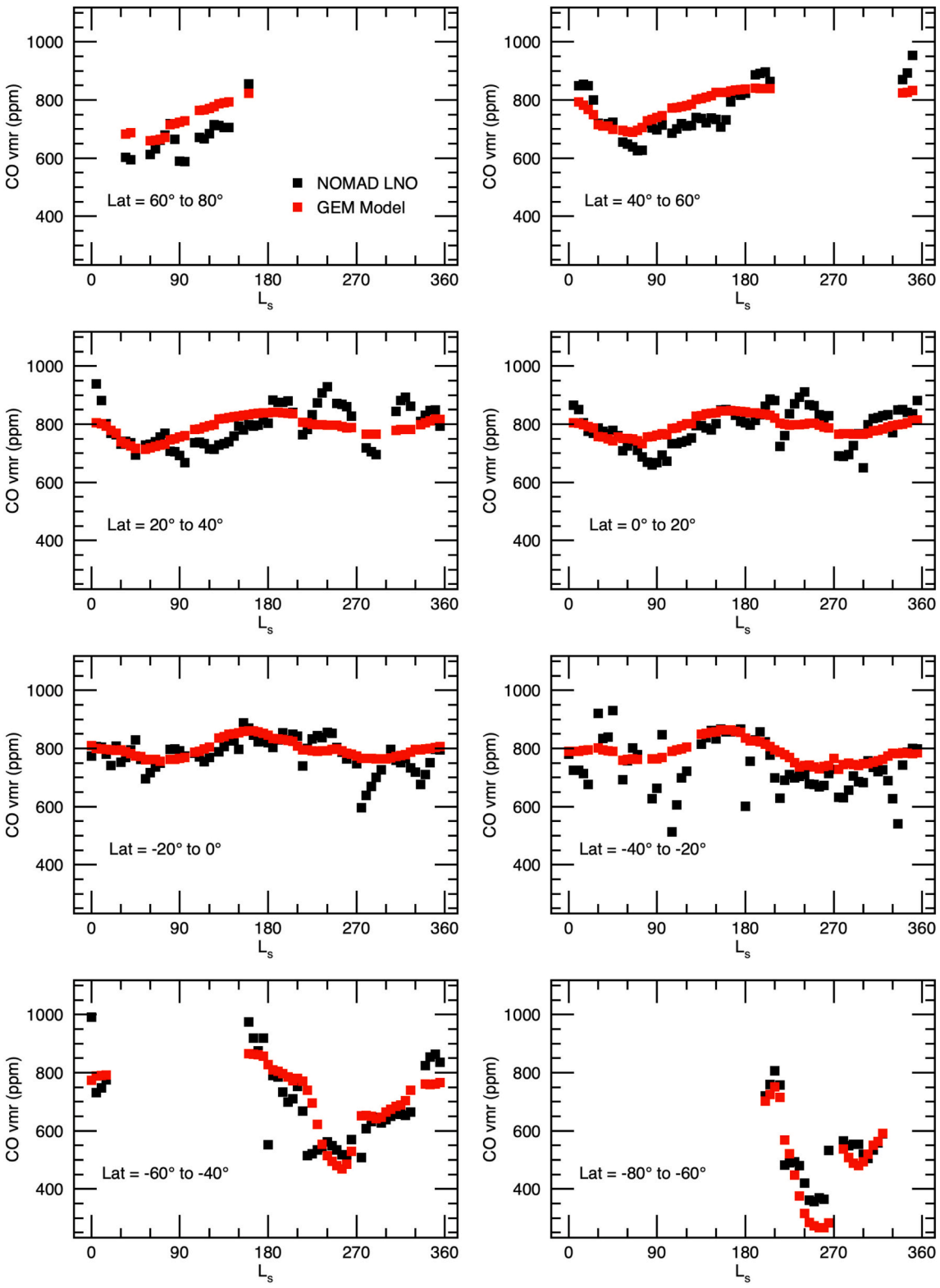

Fig. 11. Comparison of GEM-Mars model simulation of CO vmr (red points) with NOMAD LNO retrievals of CO vmr (black points). Both datasets have been binned 15° in L_s. (For interpretation of the references to colour in this figure legend, the reader is referred to the web version of this article.)

In general, the GEM-Mars General Circulation Model can reproduce the relative distribution of the observed climatology of CO vmr and explain its broad features (Daerden et al., 2019). Carbon monoxide is a relatively long-lived (~6 years; Krasnopolsky, 2007) and non-condensable species. As such, we do not expect significant interannual variations, and the column-averaged volume mixing ratio of CO is controlled by the condensation of CO_2 and latitudinal transport. The condensation of CO_2 onto the southern seasonal cap during winter is followed by this CO-enriched air being transported equatorward and into the northern hemisphere between $L_s = 120°$ and 180° forming the low-latitude maximum in CO vmr that is observed. Sublimation of the seasonal CO_2 cap during Spring and Summer releases large amounts of

CO_2 leading to a minimum in CO vmr. The amount of CO_2 condensed onto the southern cap is much greater than that condensed onto the northern cap, which explains the difference in the amplitude of the two summertime minima in CO vmr. Assimilation of the CO climatology observed by NOMAD LNO could help improve the parameterization of model processes and thereby reduce the difference between the model and retrieval results, which is the subject of active research.

6. Summary

The nadir-geometry LNO observations taken by the NOMAD instrument enable the characterization of the climatology of the column-averaged volume mixing ratio of carbon monoxide gas in the Martian atmosphere. Comparison of these retrieved values with the results from the GEM-Mars GCM model allow for physical interpretation of the retrieved seasonal and spatial variations, and also serve to highlight possible areas for improvement in both the model and the retrieval process.

NOMAD LNO observations taken covering more than one full Martian Year reveal the same general climatological trends that have been observed by other spacecraft (e.g., Smith et al., 2009, 2018; Bouche et al., 2021), but with some differences. The global, annual average value of CO vmr is found to be ~800 ppmv for the daylight portions of Mars observable by the NOMAD LNO observations. A minimum in CO vmr is observed at high latitudes around the summer solstice in both hemispheres, although the decrease in CO vmr is much more pronounced in the south than in the north because of the greater amount of CO_2 released from the seasonal cap in the south. At low latitudes, the seasonal trend generally follows that expected of a non-condensable gas (e.g., Forget et al., 2008; Daerden et al., 2019; Holmes et al., 2019) with maximum CO vmr in the season around $L_s = 180^\circ$ as air enriched with CO is transported northward across the equator. Maps of CO vmr show relatively little spatial variation outside of a noticeable enhancement over Hellas and other areas of low-lying topography during southern summer. There is no obvious trend in CO vmr as a function of local time for the daytime hours observed by NOMAD LNO. Compared to retrievals of CO vmr from CRISM (Smith et al., 2018), the NOMAD results show less overall variation with the high-latitude summer minima in each hemisphere having an amplitude roughly half as large.

Model results of CO vmr from the GEM-Mars GCM model broadly agree with the NOMAD LNO retrievals. The correspondence is closer than that between the GEM-Mars results and the CRISM retrievals of CO vmr (Smith et al., 2018), capturing both the amplitude of the high-latitude summertime minima and low-latitude seasonal variations observed by NOMAD. Small differences between the model and retrievals may be reduced with further improvement in model parameterizations.

The ExoMars Trace Gas Orbiter and NOMAD instrument continue to operate at the time of this writing taking new LNO observations in orders 189 and 190 to characterize CO. Further observations will extend the existing record of carbon monoxide retrievals to provide an even better estimate of CO climatology through better statistics and by filling in the gaps between lobes seen in Fig. 10, and will enable the study of the limits of interannual variation in CO and the response of CO to large dust storms.

Declaration of Competing Interest

None.

Acknowledgements

This work was supported by NASA's Mars Program Office under WBS 604796, "Participation in the TGO/NOMAD Investigation of Trace Gases on Mars." The NOMAD experiment is led by the Royal Belgian Institute for Space Aeronomy (IASB-BIRA), assisted by Co-PI teams from Spain (IAA-CSIC), Italy (INAF-IAPS), and the United Kingdom (Open University). This project acknowledges funding by the Belgian Science Policy Office (BELSPO), with the financial and contractual coordination by the ESA Prodex Office (PEA 4000103401, 4000121493), by Spanish Ministry of Science and Innovation (MCIU) and by European funds under grants PGC2018-101836-B-I00 and ESP2017-87143-R (MINECO/FEDER), as well as by UK Space Agency through grants ST/V002295/1, ST/P001262/1, ST/R001405/1 and ST/R00145X/1 and Italian Space Agency through grant 2018-2-HH.0. This work was supported by the Belgian Fonds de la Recherche Scientifique – FNRS under grant number 30442502 (ET_HOME). The IAA/CSIC team acknowledges financial support from the State Agency for Research of the Spanish MCIU through the 'Center of Excellence Severo Ochoa' award for the Instituto de Astrofísica de Andalucía (SEV-2017-0709). US investigators were supported by the National Aeronautics and Space Administration. Canadian investigators were supported by the Canadian Space Agency."

References

Thomas, I., et al., 2020. Radiometric calibration of NOMAD observations (In preparation).
Aoki, S., Vandaele, A.C., Daerden, F., et al., 2019. Water vapor vertical profiles on Mars in dust storms observed by TGO/NOMAD. J. Geophys. Res. Planets 124, 3482–3497.
Billebaud, F., Brillet, J., Lellouch, E., et al., 2009. Observations of CO in the atmosphere of Mars with PFS onboard Mars express. Planet. Space Sci. 57, 1446–1457.
Bouche, J., Coheur, P.-F., Giuranna, M., Wolkenberg, P., Nardi, L., Amoroso, M., Vandaele, A.C., Daerden, F., Neary, L., Bauduin, S., 2021. Seasonal and spatial variability of carbon monoxide (CO) in the Martian atmosphere from PFS/MEX observations. J. Geophys. Res. 126 https://doi.org/10.1029/2020JE006480.
Christensen, P.R., Bandfield, J.L., Hamilton, V.E., et al., 2001. The Mars global surveyor thermal emission spectrometer experiment: investigation description and surface science results. J. Geophys. Res. 106, 23,823–23,871.
Clancy, R.T., Muhleman, D.O., Jakosky, B.M., 1983. Variability of carbon monoxide in the Mars atmosphere. Icarus 55, 282–301.
Clancy, R.T., Muhleman, D.O., Berge, G.L., 1990. Global changes in the 0–70 km thermal structure of the Mars atmosphere derived from 1975 to 1989 microwave CO spectra. J. Geophys. Res. 95, 14543–14554.
Neary, L., Daerden, F., 2018. The GEM-Mars general circulation model for Mars: description and evaluation. Icarus 300, 458–476. https://doi.org/10.1016/j.icarus.2017.09.028.
Daerden, F., Whiteway, J.A., Neary, L., et al., 2015. A solar escalator on Mars: self-lifting of dust layers by radiative heating. Geophys. Res. Lett. 42, 73197326. https://doi.org/10.1002/2015GL064892.
Daerden, F., Neary, L., Viscardy, S., García Muñoz, A., Clancy, R.T., Smith, M.D., Encrenaz, T., Fedorova, A., 2019. Mars atmospheric chemistry simulations with the GEM-Mars general circulation model. Icarus 326, 197–224.
Encrenaz, T., Fouchet, T., Melchiorri, R., et al., 2006. Seasonal variations of the Martian CO over Hellas as observed by OMEGA/Mars express. Astron. Astrophys. 459, 265–270.
Forget, F., Hourdin, F., Fournier, R., Hourdin, C., Talagrand, O., 1999. Improved general circulation models of the Martian atmosphere from the surface to above 80 km. J. Geophys. Res. 104 (E10), 24,155–24,175.
Forget, F., Millour, E., Montabone, L., Lefèvre, F., 2008. Non condensable gas enrichment and depletion in the Martian polar regions. In: Paper Presented at Third International Workshop on the Mars Atmosphere: Modeling and Observations. Lunar and Planet. Inst., Williamsburg, Va, 10–13 Nov.
Goody, R.M., Yung, Y.L., 1989. Atmospheric Radiation: Theoretical Basis. Oxford Univ Press, New York.
Gordon, L.E., Rothman, L.S., Hill, C., et al., 2017. The HITRAN2016 molecular spectroscopic database. J. Quant. Spectrosc. Rad. Transf. 203, 3–69.
Guzewich, S.D., Lemmon, M., Smith, C.L., et al., 2018. Mars science laboratory observations of the 2018/Mars year 34 global dust storm. Geophys. Res. Lett. 46 https://doi.org/10.1029/2018GL080839.
Holmes, J.A., Lewis, S.R., Patel, M.R., Smith, M.D., 2019. Global analysis and forecasts of carbon monoxide on Mars. Icarus 326, 232–245.
Holmes, J.A., Lewis, S.R., Patel, M.R., 2020. OpenMARS: a global record of martian weather from 1999 to 2015. Planet. Space Sci. 188, 104969. https://doi.org/10.1016/j.pss.2020.104962.
Kaplan, L.D., Connes, J., Connes, P., 1969. Carbon monoxide in the Martian atmosphere. Astrophys. J. 157, L187–L192.
Korablev, O., Vandaele, A.C., Montmessin, F., et al., 2019. No detection of methane on Mars from early ExoMars trace gas orbiter observations. Nature 568, 517–520. https://doi.org/10.1038/s41586-019-1096-4.
Krasnopolsky, V.A., 2003. Spectroscopic mapping of Mars CO mixing ratio: detection of north-south asymmetry. J. Geophys. Res. 108, 5010. https://doi.org/10.1029/2002JE001926.
Krasnopolsky, V.A., 2007. Long-term spectroscopic observations of Mars using IRTF/CSHELL: mapping of O_2 dayglow, CO, and search for CH4. Icarus 190, 93–102.

Lacis, A.A., Oinas, V., 1991. A description of the correlated-k distribu- tion method for modeling nongray gaseous absorption, thermal emission, and multiple scattering in vertically inhomogeneous atmospheres. J. Geo Phys. Res. 96, 9027–9063.

Lefèvre, F., Krasnopolsky, V., 2017. Atmospheric Photochemistry, Chapter 13 in "The Atmosphere and Climate of Mars". Cambridge University Press. https://doi.org/10.1017/9781139060172.013.

Lellouch, E., Paubert, G., Encrenaz, T., 1991. Mapping of CO millimeter-wave lines in Mars atmosphere: the spatial distribution of carbon monoxide on Mars. Planet. Space Sci. 39, 219–224.

Lian, Y., Richardson, M.I., Newman, C.E., Lee, C., Toigo, A.D., Mischna, M.A., Campin, J.-M., 2012. The Ashima/MIT Mars GCM and argon in the martian atmosphere. Icarus 218, 1043–1070. https://doi.org/10.1016/j.icarus.2012.02.012.

Liuzzi, G., Villanueva, G.L., Mumma, M.J., Smith, M.D., Daerden, F., Ristic, B., Thomas, I., Vandaele, A.C., Patel, M.R., Lopez-Moreno, J.-J., Bellucci, G., the NOMAD team, 2019. Methane on Mars: new insights into the sensitivity of CH_4 with the NOMAD/ExoMars spectrometer through its first in-flight calibration. Icarus 321, 671–690.

Martínez, G.M., Newman, C.N., Vicente-Retortillo, Á., et al., 2017. The modern near-surface Martian climate: a review of in-situ meteorological data from Viking to Curiosity. Space Sci. Rev. https://doi.org/10.1007/s11214-017-0360-x.

Millour, E., Forget, F., Spiga, A., Vals, M., Zakharov, V., Montabone, L., Lefèvre, F., Montmessin, F., Chaufray, J.-Y., López-Valverde, M.A., González-Galindo, F., Lewis, S.R., Read, P.L., Desjean, M.-C., Cipriani, F., the MCD development team, 2018. The Mars Climate Database (version 5.3). Presented at the "From Mars Express to ExoMars" Scientific Workshop, 27–28 February 2018, Madrid, Spain.

Montabone, L., Forget, F., Millour, E., Wilson, R.J., Lewis, S.R., Cantor, B., Kass, D., Kleinböhl, A., Lemmon, M.T., Smith, M.D., Wolff, M.J., 2015. Eight-year climatology of dust optical depth on Mars. Icarus 251, 65–95.

Montabone, L., Spiga, A., Kass, D.M., Kleinböhl, A., Forget, F., Millour, E., 2020. Martian Year 34 column dust climatology from Mars Climate Sounder Observations: reconstructed maps and model simulations. J. Geophys. Res. 125 e2019JE006111.

Moreno, R., Lellouch, E., Forget, F., Encrenaz, T., Guilloteau, S., Millour, E., 2009. Wind measurements in the Mars' middle atmosphere: IRAM Plateau de Bure interferometric CO observations. Icarus 201, 549–563.

Clancy, R.T., Wolff, M.J., Christensen, P.R., 2003. Mars aerosol studies with the MGS-TES emission phase function observations: optical depths, particle sizes, and ice cloud types versus latitude and solar longitude, J. Geophys. Res., 108(E9), 5098, doi: https://doi.org/10.1029/2003JE002058.

Neary, L., Daerden, F., Aoki, S., Whiteway, J., Clancy, R. T., Smith, M., et al., 2020. Explanation for the increase in high-altitude water on Mars observed by NOMAD during the 2018 global dust storm. Geophys. Res. Lett., 47, e2019GL084354, doi: 10.109/2019GL084354.

Nevejans, D., Neefs, E., Van Ransbeeck, E., Berkenbosch, S., Clairquin, R., De Vos, L., Moelans, W., Glorieux, S., Baeke, A., Korablev, O., Vinogradov, I., Kalinnikov, Y., Bach, B., Dubois, J.P., Villard, E., 2006. Compact high-resolution space-borne echelle grating spectrometer with AOTF based on order sorting for the infrared domain from 2.2 to 4.3 micrometer. Appl. Opt. 45, 5191–5206.

Patel, M.R., Antoine, P., Mason, J.P., Leese, M.R., Hathi, B., Stevens, A.H., Dawson, D., Gow, J.P.D., Ringrose, T.J., et al., 2017. NOMAD spectrometer on the ExoMars trace gas orbiter mission: part 2 – design, manufacturing, and testing of the ultraviolet and visible channel. Appl. Opt. 56, 2771–2782.

Sindoni, G., Formisano, V., Geminale, A., 2011. Observations of water vapour and carbon monoxide in the Martian atmosphere with the SWC of PFS/MEX. Planet. Space Sci. 59, 149–162.

Smith, M.D., 2018. Local time variation of water ice clouds on Mars as observed by THEMIS. Icarus 333, 273–282.

Smith, M.D., 2019. THEMIS observations of the 2018 Mars global dust storm. J. Geophys. Res. Planets 124. https://doi.org/10.1029/2019JE006107.

Smith, M.D., Wolff, M.J., Clancy, R.T., Murchie, S.L., 2009. Compact Reconnaissance Imaging Spectrometer observations of water vapor and carbon monoxide. J. Geophys. Res. 114, E00D03 https://doi.org/10.1029/2008JE003288.

Smith, M.D., Daerden, F., Neary, L., Khayat, A., 2018. The climatology of carbon monoxide and water vapor on Mars as observed by CRISM and modeled by the GEM-Mars general circulation model. Icarus 301, 117–131.

Thomas, G.E., Stamnes, K., 1999. Radiative Transfer in the Atmosphere and Ocean. Cambridge Univ. Press, Cambridge.

Tillman, J.E., Johnson, N.C., Guttorp, P., Percival, D.B., 1993. The Martian annual atmospheric pressure cycle: years without great dust storms. J. Geophys. Res. 98 (E6), 10963–10971.

Titov, D.V., Svedhem, H., McCoy, D., et al., 2006. Venus express: scientific goals, instrumentation and scenario of the mission. Cosm. Res. 44, 334–348.

Vandaele, A.C., Neefs, E., Drummond, R., et al., 2015. Science objectives and performances of NOMAD, a spectrometer suite for the ExoMars TGO mission. Planet. Space Sci. 119, 233–249.

Vandaele, A.C., Lopez-Moreno, J.-J., Patel, M.R., et al., 2018. NOMAD, an integrated suite of three spectrometers for the ExoMars trace gas Mission: technical description, science objectives and expected performance. Space Sci. Rev. 214, 80. https://doi.org/10.1007/s11214-018-0517-2.

Vandaele, A.C., Korablev, O., Daerden, F., et al., 2019. Martian dust storm impact on atmospheric H_2O and D/H observed by ExoMars trace gas orbiter. Nature 568, 521–525. https://doi.org/10.1038/s41586-019-1097-3.

Vincente-Retortillo, Á., Martínez, G.M., Renno, N.O., Lemmon, M.T., de la Torre-Juárez, M., 2017. Determination of dust aerosol particle size at Gale crater using REMS UVS and Mastcam measurements. Geophys. Res. Lett. 44 https://doi.org/10.1002/2017GL072589.

Wolff, M.J., Clancy, R.T., 2003. Constraints on the size of martian aerosols from thermal emission spectrometer observations. J. Geophys. Res. 108, 5097. https://doi.org/10.1029/2003JE002057.

Wolff, M.J., et al., 2006. Constraints on dust aerosols from the Mars Exploration Rovers using MGS overflights and Mini-TES. J. Geophys. Res. 111, E12S17 https://doi.org/10.1029/2006JE002786.

Wolff, M.J., et al., 2009. Wavelength dependence of dust aerosol single scattering albedo as observed by the Compact Reconnaissance Imaging Spectrometer. J. Geophys. Res. 114, E00D04 https://doi.org/10.1029/2009JE00350.